Spectrochimica Acta Part A: Molecular and Biomolecular Spectroscopy 327 (2025) 125336

Contents lists available at ScienceDirect

Spectrochimica Acta Part A:
Molecular and Biomolecular Spectroscopy

journal homepage: www.journals.elsevier.com/spectrochimica-acta-part-a-molecular-and-biomolecular-spectroscopy

Atropisomerism of diflunisal unveiled by rotational spectroscopy and quantum chemical calculations

Andrés Verde [a,*], Susana Blanco [a], Juan Carlos López [a], Francisco Gámez [b,*]

[a] Department of Physical Chemistry, IU CINQUIMA Facultad de Ciencias, Universidad de Valladolid, Paseo Belén 7, 47011 Valladolid, Spain
[b] Department of Physical Chemistry, Universidad Complutense de Madrid, 28040 Madrid, Spain

HIGHLIGHTS

- The full conformational space of diflunisal is investigated by quantum chemistry calculations.
- Laser-ablation microwave spectroscopy is used to identify the most stable conformer of diflunisal.
- Atropisomeric features are related with reported structures of solid complexed proteins.

GRAPHICAL ABSTRACT

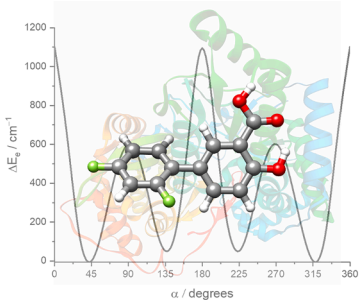

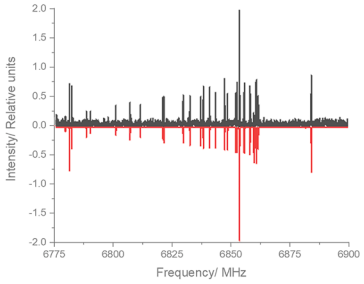

ARTICLE INFO

Keywords:
Rotational spectroscopy
Molecular structure
Atropisomers
Non-steroideal anti-inflammatory drugs

ABSTRACT

The most stable conformer of laser-ablated diflunisal has been isolated in a supersonic expansion and experimentally detected through high-resolution chirped-pulse rotational spectroscopy. State-of-the-art chemical calculations allowed to understand the nature of the strong stabilization of the detected conformer and its atropisomer among a total of sixteen theoretically predicted conformers and confirmed the presence of a resonance assisted hydrogen bond (RAHB) between the hydroxyl hydrogen atom and the carbonyl oxygen atom of the carboxylic acid group. The comparison of the experimental data from this work and the information found in the literature about the molecule in condensed phases corroborates the existence of these two atropisomers and is contextualized within the complexation arrangement of diflunisal with relevant proteins.

1. Introduction

Chirality has an extremely important role in drug discovery and development since it is well established that enantiomers can differ significantly in their biological and pharmacological properties [1]. Recent research works are focused on the pharmaceutical implications of a clearly overlooked source of drug chirality, atropisomerism, which is closely related to axial chirality resulting from the rotation around a single bond [2]. Although classical chiral compounds are often stable and need a bond breaking and making process to racemize, atropisomers racemize through an intramolecular dynamic process that just involves bond rotation, giving rise to half-lives that can go from seconds to years [3].

Biphenyl derivatives, which are common moieties in drugs due to

* Corresponding authors.
E-mail addresses: andres.verde@uva.es (A. Verde), frgamez@ucm.es (F. Gámez).

https://doi.org/10.1016/j.saa.2024.125336
Received 3 June 2024; Received in revised form 18 October 2024; Accepted 22 October 2024
Available online 24 October 2024

their inherent properties, give rise to axial chirality and atropisomerism through the rotation around the single bond linking the phenyl rings. These biphenyl moieties are present in some of the most used non-steroidal anti-inflammatory drugs (NSAIDs), such as flurbiprofen and diflunisal. For instance, the combination of atropisomerism and chirality has been observed to play an important role in the recognition of flurbiprofen by proteins [4]. This behavior was unveiled by the comparison of gas-phase information obtained through rotational spectroscopy with condensed-phase data found in literature when flurbiprofen complexed with cyclooxygenase enzymes. Although for diflunisal there is a huge amount of valuable information about its structure complexed with proteins [5–8], there is not an experimental work on the isolated molecule that could provide essential information on its inherent properties that would improve the knowledge about this drug.

Diflunisal, which is a white solid derived from salicylic acid by a 2,4-difluorophenyl substitution at the 5-position (see Fig. 1), acts as a cyclooxygenase-2 inhibitor, having potent anti-inflammatory, analgesic, uricosuric and antipyretic properties. In addition, it is used to relieve pain in patients with rheumatoid arthritis and osteoarthritis. However, it is also worth mentioning that this drug increases the risk of heart attacks [9,10].

Since the boiling point of diflunisal is reasonably high (~210 °C), the inquiry into the dominant conformation in the gas phase can be addressed using laser ablation rotational spectroscopy in combination with appropriate quantum chemical calculations. Such procedure allows to unequivocally locate the observed rotamers in the potential energy surface (PES) wells identifying the different stable conformations. Good examples are the rotational spectroscopy works done for flurbiprofen [4], ibuprofen [11], thalidomide [12] or paracetamol [13].

Even though the conformer identification is performed in isolated conditions, this methodology helps in elucidating (i) if the structures of the drug found in the solid state can be related to the most stable conformers in the gas phase; (ii) if so, to understand the intrinsic molecular features that lead to the supramolecular recognition in the protein active and/or allosteric center from first principles approaches. Herein, we will apply this method to describe the configurational, energetic and protein interaction preferences of diflunisal under isolated conditions. Such elucidation is put in the context of the interaction of this drug with different proteins related to its biochemical activity.

2. Experimental section

The rotational spectrum of diflunisal has been recorded in the 2–8 GHz region employing the laser-ablation chirped-pulse Fourier transform microwave (LA-CP-FTMW) spectrometer located at University of Valladolid and described elsewhere [14,15]. A solid rod of the sample was prepared by grinding and compressing a 1:1 weight ratio mixture of the commercial sample of diflunisal and Cu powder. The rod sample is continuously translating and rotating while being vaporized by laser pulses of 532 nm, 5.2 ns pulse width and energy of 20 mJ per pulse from a Q-switch Nd/YAG laser (Quantel Q-smart 850). The ablation plume was dragged by using Ar as carrier gas at a stagnation pressure of 2 bar forming a jet expansion into the high vacuum chamber. Then, a 4 μs microwave chirp pulse (covering the 2–8 GHz region), generated by an arbitrary wavefunction generator and amplified up to 200 W by a TWT amplifier, was broadcasted into the vacuum chamber through a horn antenna to excite the molecules in the jet. The subsequent free induction decay (FID) signal was collected through a second horn antenna, amplified and recorded in the time domain by a digital oscilloscope and Fourier-transformed to the frequency domain. The polarization-detection sequence frame was repeated up to eight times per molecular expansion pulse, obtaining as a result a total of eight averaged spectra in every molecular pulse. The repetition rate used in this experiment was 5 Hz to allow optimal vacuum conditions. Under these conditions a total of approximately 10^6 spectra were accumulated. The accuracy of frequency measurements is estimated to be better than 15 kHz.

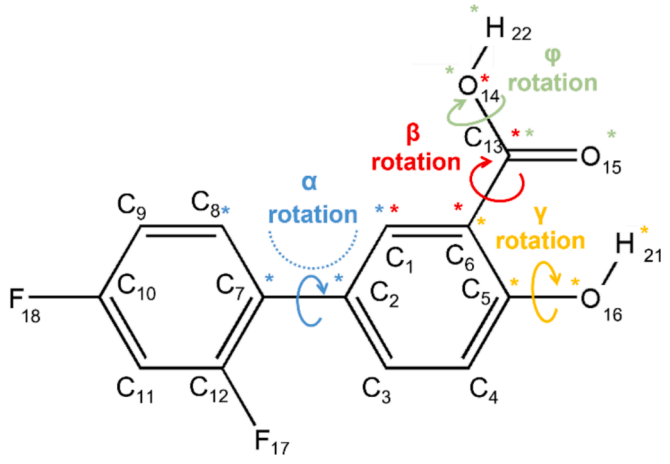

Fig. 1. Atom labelling for diflunisal. The potential characteristic rotations are also shown.

3. Theoretical methods

The conformational investigation of diflunisal was carried out by exploring its potential energy surface (PES) using the Conformer-Rotamer Ensemble Sampling Tool (CREST) [16] and following chemical intuition. The molecular structures of all the possible conformations were further optimized using the B3LYP hybrid functional [17] with the D3 Grimme's empirical dispersion correction [18] and Pople's 6-311++G(d,p) basis set [19]. Harmonic approximation calculations were done to verify that the obtained conformers were indeed minima in the PES and to obtain the Gibbs energy. Moreover, the harmonic approximation calculations have also allowed us to estimate the quartic centrifugal distortion constants and the zero-point corrected energies. The interconversion barriers were calculated with relaxed scans around the dihedral angles that define the molecule and with the Synchronous Transit Quasi- Newton (STQN) method [20] developed by Schlegel and Peng, that locate the corresponding transition states, at the B3LYP-D3/6-311++G(d,p) level. Additional theoretical calculations were performed for the two most stable conformers with the range-separated functional ωB97xD [21], *ab initio* MP2 method and M06-2X [22] level with the 6-311++G(d,p), aug-cc-pVTZ and def2TVZP basis sets. All calculations were performed using the GAUSSIAN16 package [23].

Non-covalent interaction (NCI) [24], Bader's quantum theory of atoms in molecules (QTAIM) [25] and natural bond orbital (NBO) [26] analysis were done to provide insights about the possible intramolecular interactions that stabilize the conformers.

4. Results

4.1. Conformational landscape

Diflunisal is a flexible molecule that can adopt several conformations defined by the dihedral angles α (C_1–C_2–C_7–C_8), β (C_1–C_6–C_{13}–O_{14}), γ (C_6–C_5–O_{16}–H_{21}) and ϕ (O_{15}–C_{13}–O_{14}–H_{22}) (see Fig. 1). Relaxed scans around all these dihedral angles give rise to a total of 16 possible conformations in an electronic energy window of ~6000 cm^{-1} (see Fig. S1 and Table S1 for structural details of the conformers) labeled from C1 to C16 based on their relative electronic energies. Overall, these conformers can be organized in eight pairs of conformers with a difference in the relative disposition of the 2,4′-difluorobiphenyl moiety that is defined by α. The conformers within a pair are atropisomers because of the rotation of the 2,4-difluorobiphenyl moiety about the C_2—C_7 single bond. The calculated energies indicate that although the conformational

space may occur around the rotation of the mentioned dihedral angles, the flexibility due to the rotational degrees of freedom is restricted to conformations maximizing the intramolecular hydrogen bond (HB) between the carboxyl and hydroxyl groups at *ortho*-position.

The two most stable atropisomers, C1 (α = ±42.48°) and C2 (α = ±136.73°), exhibit the intramolecular HB and have a relative electronic energy difference between them of just 54 cm^{-1} calculated at B3LYP-D3/6-311++G(d,p) level of theory (see Tables S2 and S3 for the equilibrium structures). Considering vibrational effects, we have calculated the zero-point corrected energy and Gibbs energy of C2 relative to C1, to be 52 cm^{-1} and 46 cm^{-1} respectively. Moreover, all the additional theoretical methods used also predict C1 as the global minimum (see Tables S4–S6). The potential energy function describing the difluorobiphenyl torsion that interconverts these two conformers is shown in Fig. 2. The minima with the highest interconversion barriers are conformational enantiomers, i.e., they own identical rotational constants different sign of the dipole moment components. Consequently, conformational enantiomers are indistinguishable in terms of rotational spectroscopy. The C1-to-C2 interconversion barrier is 549.5 cm^{-1} using electronic energies and 606.3 cm^{-1} using the energies of the transition states located using the STQN method. The minor energy differences obtained with both methods employed may be because in the potential energy function the parameter is made to vary and remain fixed at each point to avoid its relaxation to the minimum, while STQN method optimizes the transition states. Due to the value of the interconversion barrier between C1 and C2, this atropisomerism belongs to class 1 [27]. In conclusion, conformers C1 and C2 dominate the conformational space at room temperature.

4.2. Rotational spectra

The jet cooled rotational spectrum of laser-ablated diflunisal, recorded in the 2–8 GHz region, is shown in Fig. S2. In Fig. 3 we show the details of the spectrum in the 6.75–6.90 GHz range. From the calculations, we found that all diflunisal conformers are prolate asymmetric rotors, with Ray asymmetry parameter values close to −1. A rotamer showing exclusively a *b*-type spectrum was assigned in the rotational spectrum using the set of rotational constants of the predicted

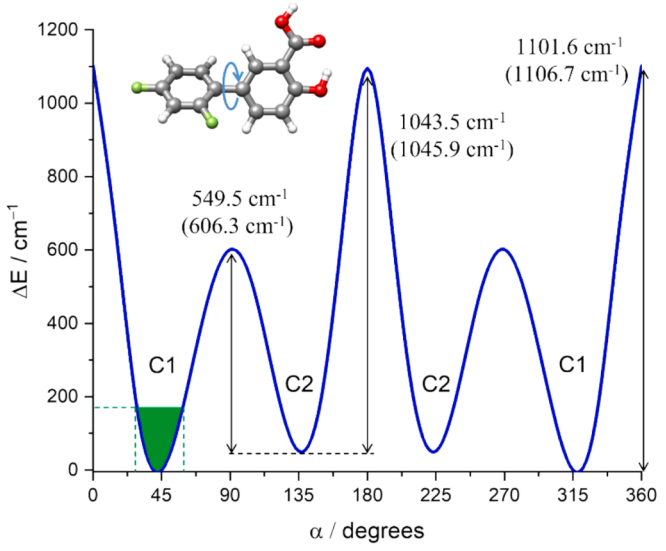

Fig. 2. Calculated B3LYP-D3/6-311++G(d,p) potential energy function around the α dihedral angle defining the difluorobiphenyl group torsion. The values in parenthesis show the interconversion barriers calculated using the STQN method at the same level of theory. The green lines indicate the range of values of α found in the C1-like structures of reported diflunisal complexes with proteins (see below).

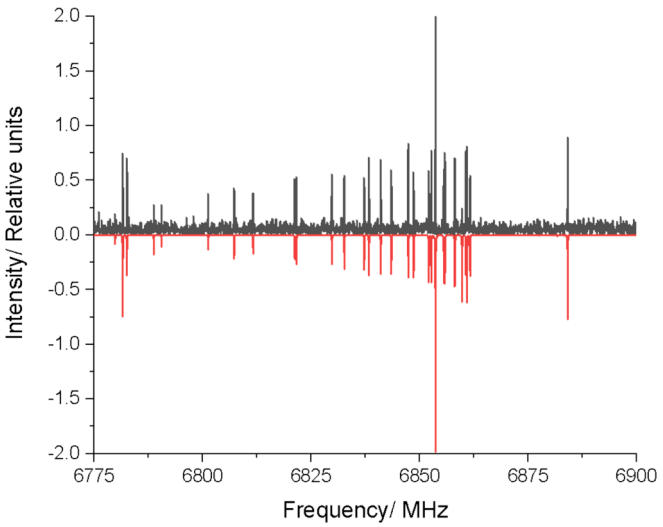

Fig. 3. A 6.75–6.90 GHz section of the CP-FTMW spectrum of laser-ablated diflunisal in black. The spectrum calculated from the experimentally determined rotational parameters for C1 is shown in red.

as most stable conformer, C1. No *a*- or *c*-type transitions were observed for assignment. Overall, a total of 142 rotational transitions were finally fitted for this rotamer using the *S*-reduced semirigid rotor Hamiltonian of Watson [28] in the I^r representation. The rotamer unequivocally matches with the relatively high-value of the μ_b component of the dipole moment of C1. On the other hand, C2 presents just a 0.1 D value of the μ_b. The relative error between the experimental and B3LYP-D3/6-311++G(d,p) theoretical rotational constants is 0.2 % for *A* and *B* rotational constants and 0.4 % for *C*. The errors are small enough to identify the rotamer with C1. It can be pointed out that all the theoretical methods predict the rotational parameters of C1 form closer to the observed than any other conformer. This shows the good agreement between the theoretical calculations and the experimental data. All the rotational transitions measured are given in Table S7. Once all the C1 transitions were measured, no additional spectral lines were available in the spectrum. Subsequently, no transitions were observed for C2 conformer.

Although a partial-relaxation of C2 into C1 could occur due to the relatively small value of the interconversion barrier (~550–600 cm^{-1}) between both forms, [29] the non-observation of C2 conformer can be alternatively explained in terms of the dipole moment components and relative abundances. For C1 only *b*-type rotational transitions have been measured (μ_b = 1.9 D), while *a*- and *c*-type transitions were not detected (μ_a = 0.4 D, μ_c = 0.5 D). The relative intensities of the transitions for C2 conformer can be approximately predicted assuming no relaxation processes occur in the supersonic jet. Laser ablation brings diflunisal molecules into the gas phase being thermalized in the region where the ablation plume crosses the expanding carrier gas jet. Assuming a situation in that region close to equilibrium at pressure and temperature lower than the stagnation ones, the subsequent expansion brings all the molecules populating both conformers to the corresponding ground vibrational states. Thus, the relative equilibrium conformer populations evaluated from the Gibbs free energy can be related to the observed intensities, which are proportional to the corresponding number densities. Considering a beam temperature of 273 K [30,31] at 2 bar, the relative intensities were calculated taking into account the line strength of the transitions, the squared vale of the electric dipole moment components and the Gibbs energy [32]. A relative abundance of the conformers in the beam of 1:0.8 was obtained and an intensity ratio of 1:2.5 for the *c*-type transitions (μ_c = 0.5 D and 0.9 D for C1 and C2 respectively). The most intense *c*-type transitions for conformer C1 not observed are below the noise. Although C2 *c*-type lines are more intense

than the corresponding to C1, C2 transitions could be around the limit of detection. The observations indicate that either the population, reduced by a total- or partial-relaxation, and dipole moments of this conformer are too low to be detected or it does not exist in our experimental conditions.

4.3. Molecular structure and intramolecular interactions

The experimental value of the planar moment P_c, which measures the mass distribution out of the *ab* plane, of the conformer C1 is 65.1507(11) uÅ^2 (see Table 1). Because of the non-planar arrangement of the difluorophenyl ring, this value is ~550 times higher than that found for salicylic acid in the gas phase, for which $P_c = 0.1262(19)$ uÅ^2 [33]. The torsional angle of the 2′,4-difluorobiphenyl moiety in C1 is predicted to be ±42.48°. It can be pointed out that the relative error committed by theoretical methods predicting P_c value with respect to the experimental one is of just 5 %. However, small changes in α dihedral angle further reduce this difference giving a more reliable structure. In this way, setting α = ±43.58° gives a set of rotational constants ($A = 950.37$ MHz; $B = 202.93$ MHz; $C = 174.76$ MHz) that result in a P_c of 65.14 uÅ^2. This value of the dihedral angle is similar to that presented in the biphenyl molecule and its derivatives. For instance, the torsional angle is ±44.4 (1.2)° for the biphenyl molecule [34], ±49 (5)° for 2-fluorobiphenyl [35] and ±44(5)° for 4,4′-difluorobiphenyl [35] in the gas phase. The value is also similar to that found for other nonsteroidal anti-inflammatory agent drugs with somewhat similar structures, e.g., this torsional angle is 44.26° for flurbiprofen [4].

The torsional angle in diflunisal and all the biphenyl derivatives is the result of an intricate balance of forces involving the π-conjugation between both rings, favoring a co-planar configuration and the steric repulsion between the adjacent atoms in *ortho*-position. In this context, NCI, NBO and QTAIM analyses have been carried out to provide insights into the possible intramolecular interactions that stabilize the detected conformer. NCI and QTAIM analysis for C1 are shown in Fig. 4. In the NCI scatter graph also shown in Fig. 4, the Y axis represents the reduced density gradient (RDG) and the X axis the sign $[\lambda_2(r)]\rho(r)$ function, being $\rho(r)$ the electron density function and $\lambda_2(r)$ is the second highest eigenvalue of the electron-density Hessian matrix. Weak interactions have positive correlation with the electron density in the corresponding region. On the other hand, van der Waals interaction regions present very low values of $\rho(r)$. Regions corresponding to hydrogen bonding and strong steric effects have larger values of $\rho(r)$. A positive sign of $\lambda_2(r)$ indicates repulsive interactions, while negative values represent attractive interactions. The product of the sign of both $\lambda_2(r)$ and $\rho(r)$ allows the visualization of non-covalent interactions. The spikes in the low part of the graph represent the non-covalent interactions of the system. Those on the left part are attractive interactions and those of the right part correspond to repulsive interactions.

As expected, the most significant interaction observed in the detected conformer is a strong intramolecular HB, depicted in blue in the NCI plot and established between the hydrogen atom of the hydroxyl group and the carbonyl oxygen atom of the carboxylic acid group. The predicted distance at the B3LYP-D3/6-311++G(d,p) level of theory is 1.776 Å. QTAIM analysis reveals the existence of a (3, −1) bond critical point (BCP) between these two atoms. The formation of the six-membered ring through the intramolecular HB is also observed as a (3, +1) ring critical point (RCP). Taking into account that the electronic density is related to the strength of the bond, the interaction energy for the intramolecular HB in C1 is estimated to be −8.13 kcal mol^{-1} [30]. NBO calculations reflect this interaction predicting an electron density transfer from the O_{15} lone pair to the O_{16}–H_{21} antibonding σ* orbital with a second order $E^{(2)}$ energy of 3.20 kcal mol^{-1}. Given the strength of this interaction, these analyses support the hypothesis that the intramolecular HB is further stabilized by resonance assisted hydrogen bonding (RAHB), similar to the behavior observed in salicylic acid [27]. Similar but weaker HB interactions have been observed in the high energy conformers C3, C4, C5 and C6. Furthermore, all diflunisal conformers exhibit a weak CH···F intramolecular HB between the polar fluorine atom and the closest hydrogen atom in the adjacent phenyl ring, contributing to the stabilization of the structures. Particularly, the CH···F distance is 2.485 Å in C1. The interaction energy obtained from the electronic density has a value of −1.58 kcal mol^{-1}. QTAIM also reveals that there is a (3, +1) RCP that shows the HB closing a *pseudo* six-membered ring. In the flurbiprofen molecule, the CH···F is 2.482 Å and the stabilization energy is −1.56 kcal mol^{-1} [5]. Additional weaker attractive interactions, such as the interaction between the carboxylic functional group and the closest hydrogen of the phenyl ring are also revealed by NCI. In C1 conformer, the H···OH predicted distance between both atoms is 2.400 Å. Additionally, our NCI calculations show that there is an H···H attractive interaction between the closest hydrogen atoms of the difluorobiphenyl moiety, with a predicted distance of 2.453 Å.

Table 1
Rotational parameters obtained from the analysis of the spectrum of the C1 conformer of diflunisal and its comparison with the DFT values (B3LYP-D3/6-311++G(d,p)) for the identified form.

Param.[a]	Experimental values	DFT values
A/MHz	952.01848(10)[b]	950.29
B/MHz	203.574986(72)	203.12
C/MHz	175.292044(72)	174.55
κ	−0.93	−0.93
P_a/uÅ^2	2417.3699(11)	2425.80
P_b/uÅ^2	465.6994(11)	469.53
P_c/uÅ^2	65.1507(11)	62.29
D_J/kHz	0.00167(13)	0.001249
D_{JK}/kHz	–	0.06409
D_K/kHz	–	0.00365
d_1/kHz	–	−0.00016
d_2/kHz	–	−0.00009
σ/kHz	4.0	–
N	142	–
μ_a/D	No	0.4
μ_b/D	Yes	−1.9
μ_c/D	No	−0.5

[a] A, B and C are the rotational constants; κ is Ray's asymmetry parameter ($\kappa = (2B - A - C)/(A - C)$); P_α ($\alpha = a$, b or c) are the planar moment of inertia derived from the inertial moments I_α ($P_c = (I_a + I_b - I_c)/2$); D_J, D_{JK}, D_K, d_1 and d_2 are the quartic centrifugal distortion constants; σ is the rms deviations of the fit; N is the number of lines fitted; μ_a, μ_b, and μ_c, are the components of the electric dipole moment along the principal inertial axes. Yes/No indicate if selection rules governed by that dipole moment component have been observed.

[b] Standard errors are given in parentheses in units of the last digit.

4.4. Comparison with condensed-phase data

It is of chemical and biological interest to compare the observed conformation in the gas phase with those previously reported for diflunisal in condensed phases. The gas-phase structure C1 detected in this work matches with two structures, A1 and A2, found by Cross *et al.* [36] using X-ray diffraction techniques for solid diflunisal. In such structures, the α dihedral angle seems to have a slightly lower value in diflunisal in the condensed phases while the γ dihedral angle is slightly higher. Another diflunisal structure (B) detected by Cross *et al.* [36] corresponds to the C2 conformer. The C1 and C2 values of the dihedral angles that define the molecule are compared to those of the condensed phases in Table 2.

Because of the pharmaceutical activity that diflunisal presents, the gas phase structure can be compared with that presented when complexed with proteins. Although its more common therapeutical effect occurs by the inhibition of the prostaglandin-endoperoxide synthase, among the set of molecular structures stored in the Protein Data Bank [37] and to our knowledge, none of the reported structures contemplate such binding. Furthermore, in all the structures, diflunisal is present in

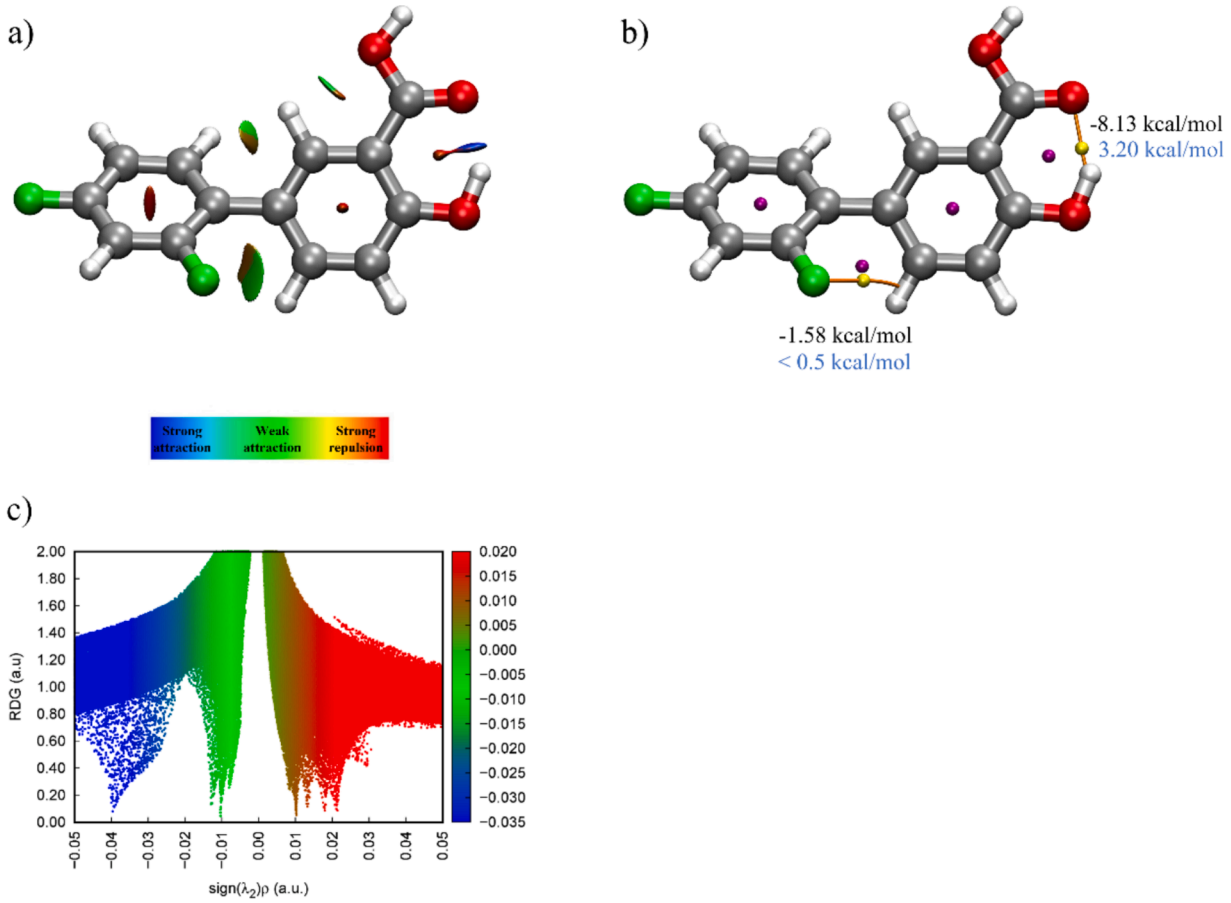

Fig. 4. a) NCI plot maps the location and strength of intramolecular interactions with coloured isosurfaces ranging from blue (strong attraction) to red (strong repulsion) according to the product of the sign of the second eigenvalue of the Hessian and electron density. b) QTAIM analysis plot shows (3, −1) bond critical points in yellow, (3, +1) ring critical points in purple and bond paths in orange. The interaction energy in black has been calculated from the values of the QTAIM analysis and the energies in blue have been extracted from the NBO analysis. c) Reduced density gradient (RDG) graph (explained in the text).

Table 2
Comparison of dihedral angles between gas-phase conformers predicted at B3LYP-D3/6-311++G(d,p) level of theory and X-ray data (A1, A2 and B) obtained by Cross et al. [36]. Angles are given in degrees.

Parameter	C1	A1	A2	C2	B
α (C–C–C–C)	±43.58	−40.63	38.86	±136.73	−136.51
β (C–C–C–O)	−0.47	0.47	−0.44	0.32	2.42
γ (C–C–O–H)	0.36	−0.67	−0.66	−0.02	0.21
ϕ (O–C–O–H)	−0.38	0.07	−0.05	0.25	2.89

an ionic form that only makes possible to compare the value of α dihedral angle. In a comparative study, the C1-like structure (α ranging ±26.96° – ±54.62°) has been reported when bound to a DNA-polymerase that inhibits the growth of *Helycobacter pylori* [5], to the α-amino-β-carboxymuconate-ε-semialdehyde decarboxylase [6] or in relation with its role as modulator of the stability of the transthyretin, a protein related with some types of amyloidosis [7]. The latter interaction can also occur in a C2-like conformation [8]. Surprisingly, this C2-arrangement is preferred when complexed with human serum albumin, a protein that, because of its strong binding energy with diflunisal, constitutes the main sink of this drug against its therapeutic effect [7,8]. All the mentioned diflunisal structures complexed with proteins are accessible from conformers C1 and C2 with a low energetic cost. For instance, the values of α for C1 can be related with structures that are found in the C1 PES well, having relative energetic values of less than 200 cm^{-1} (see Fig. 2). Overall, we conclude that the structures found for diflunisal, using the synergy of spectroscopic techniques and quantum chemical calculations resemble those reported in the complexation with biologically relevant proteins.

5. Conclusions

Despite the apparent diversity of potential conformations diflunisal can present, only two conformers, which are class-1 atropisomers, are found to be within an energy window of 100 cm^{-1}. The predicted global minimum was detected using high-resolution microwave spectroscopy coupled with supersonic jets. Due to the high boiling point and the low vapour pressure of the sample, the laser ablation method has been employed to vaporize the sample. The value of the difluorobiphenyl torsional angle observed for this diflunisal conformer is similar to those of several biphenyl derivatives, such as flurbiprofen. Intramolecular interaction analysis clearly confirms the existence of a RAHB that strongly stabilizes the two atropisomers, resulting also in a planar skeleton in the salicylic part of the drug. The comparison of our results with the available data about condensed phases shows that the solid-state structures correspond to the most stable forms in the gas phase. Furthermore, the protein database analysis shows that diflunisal structures slightly differ from the isolated atropisomers at the PES minima and correspond to structures confined in the potential energy wells. Such observation evinces the importance of fundamental studies of isolated molecules aims at interpreting molecular features that help in understanding supramolecular interactions. These facts are of particular importance in modern pharmacology when atropisomers are involved in the biochemical effects of a newly designed drug.

Declaration of competing interest

The authors declare that they have no known competing financial interests or personal relationships that could have appeared to influence the work reported in this paper.

Acknowledgements

This project has been funded by grants PID2022-136919NA-C33 of the Ministry of Science, Innovation and Universities MCIN/AEI/10.13039/501100011033. The authors also acknowledge the Ministerio de Ciencia e Innovación (PID2021-125207NB-C33) and the Junta de Castilla y León (Grant INFRARED-FEDER IR2020-1-UVa02). A.V. would like to thank the University of Valladolid and Banco Santander for his Ph.D. grant.

Appendix A. Supplementary data

Supplementary data to this article can be found online at https://doi.org/10.1016/j.saa.2024.125336.

Data availability

Data will be made available on request.

References

[1] J. Clayden, W.J. Moran, P.J. Edwards, S.R. LaPlante, The challenge of atropisomerism in drug discovery, Angew. Chem. Int. Ed. 48 (2009) 6398–6401, https://doi.org/10.1002/anie.200901719.
[2] S.R. LaPlante, P.J. Edwards, L.D. Fader, A. Jakalian, O. Hucke, Revealing atropisomer axial chirality in drug discovery, ChemMedChem 6 (2011) 505–513, https://doi.org/10.1002/cmdc.201000485.
[3] S.R. LaPlante, L.D. Fader, K.R. Fandrick, D.R. Fandrick, O. Hucke, R. Kemper, S.P. F. Miller, P.J. Edwards, Assessing atropisomer axial chirality in drug discovery and development, J. Med. Chem. 54 (2011) 7005–7022, https://doi.org/10.1021/jm200584g.
[4] A. Verde, J.C. López, S. Blanco, The role of the transient atropisomerism and chirality of flurbiprofen unveiled by laser-ablation rotational spectroscopy, Chem. Eur. J. 29 (2023), https://doi.org/10.1002/chem.202300064.
[5] P. Pandey, V. Verma, G. Gautam, N. Kumari, S.K. Dhar, S. Gourinath, Targeting the β-clamp in *Helicobacter pylori* with FDA -approved drugs reveals micromolar inhibition by diflunisal, FEBS Lett. 591 (2017) 2311–2322, https://doi.org/10.1002/1873-3468.12734.
[6] Y. Yang, T. Borel, F. de Azambuja, D. Johnson, J.P. Sorrentino, C. Udokwu, I. Davis, A. Liu, R.A. Altman, Diflunisal derivatives as modulators of ACMS decarboxylase targeting the tryptophan-kynurenine pathway, J. Med. Chem. 64 (2021) 797–811, https://doi.org/10.1021/acs.jmedchem.0c01762.
[7] Y. Wang, C. Huang, G. Liou, H. Hsueh, C. Liang, H. Tseng, S. Huang, C. Chao, S. Hsieh, S. Tzeng, A molecular basis for tetramer destabilization and aggregation of transthyretin Ala97Ser, Protein Sci. 32 (2023) e4610.
[8] J. Ghuman, P.A. Zunszain, I. Petitpas, A.A. Bhattacharya, M. Otagiri, S. Curry, Structural basis of the drug-binding specificity of human serum albumin, J. Mol. Biol. 353 (2005) 38–52, https://doi.org/10.1016/j.jmb.2005.07.075.
[9] K. Shirakawa, L. Wang, N. Man, J. Maksimoska, A.W. Sorum, H.W. Lim, I.S. Lee, T. Shimazu, J.C. Newman, S. Schröder, M. Ott, R. Marmorstein, J. Meier, S. Nimer, E. Verdin, Salicylate, diflunisal and their metabolites inhibit CBP/p300 and exhibit anticancer activity, Elife 5 (2016) e11156.
[10] P. Snetkov, S. Morozkina, R. Olekhnovich, M. Uspenskaya, Diflunisal targeted delivery systems: a review, Materials 14 (2021) 6687, https://doi.org/10.3390/ma14216687.
[11] T. Betz, S. Zinn, M. Schnell, The shape of ibuprofen in the gas phase, PCCP 17 (2015) 4538–4541, https://doi.org/10.1039/C4CP05529B.
[12] S. Blanco, A. Macario, J.C. López, The structure of isolated thalidomide as reference for its chirality-dependent biological activity: a laser-ablation rotational study, PCCP 23 (2021) 13705–13713, https://doi.org/10.1039/D1CP01691A.
[13] M. Varela, C. Cabezas, J.C. López, J.L. Alonso, Rotational spectrum of paracetamol, J. Phys. Chem. A 117 (2013) 13275–13278, https://doi.org/10.1021/jp404581z.
[14] G.G. Brown, B.C. Dian, K.O. Douglass, S.M. Geyer, S.T. Shipman, B.H. Pate, A broadband Fourier transform microwave spectrometer based on chirped pulse excitation, Rev. Sci. Instrum. 79 (2008) 053103, https://doi.org/10.1063/1.2919120.
[15] A. Verde, S. Blanco, J.C. López, The conformations of isolated gallic acid: a laser-ablation rotational study, Molecules 28 (2022) 159, https://doi.org/10.3390/molecules28010159.
[16] P. Pracht, F. Bohle, S. Grimme, Automated exploration of the low-energy chemical space with fast quantum chemical methods, PCCP 22 (2020) 7169–7192, https://doi.org/10.1039/C9CP06869D.
[17] C. Lee, W. Yang, R.G. Parr, Development of the Colle-Salvetti correlation-energy formula into a functional of the electron density, Phys. Rev. B 37 (1988) 785–789, https://doi.org/10.1103/PhysRevB.37.785.
[18] S. Grimme, J. Antony, S. Ehrlich, H. Krieg, A consistent and accurate *ab initio* parametrization of density functional dispersion correction (DFT-D) for the 94 elements H-Pu, J. Chem. Phys. 132 (2010) 154104, https://doi.org/10.1063/1.3382344.
[19] M.J. Frisch, J.A. Pople, J.S. Binkley, Self-consistent molecular orbital methods 25. Supplementary functions for Gaussian basis sets, J. Chem. Phys. 80 (1984) 3265–3269, https://doi.org/10.1063/1.447079.
[20] C. Peng, H. Bernhard Schlegel, Combining synchronous transit and quasi-newton methods to find transition states, Isr. J. Chem. 33 (1993) 449–454, https://doi.org/10.1002/ijch.199300051.
[21] J.-D. Chai, M. Head-Gordon, Systematic optimization of long-range corrected hybrid density functionals, J. Chem. Phys. 128 (2008) 084106, https://doi.org/10.1063/1.2834918.
[22] Y. Zhao, D.G. Truhlar, The M06 suite of density functionals for main group thermochemistry, thermochemical kinetics, noncovalent interactions, excited states, and transition elements: two new functionals and systematic testing of four M06-class functionals and 12 other functionals, Theor. Chem. Acc. 120 (2008) 215–241, https://doi.org/10.1007/s00214-007-0310-x.
[23] M.J. Frisch, G.W. Trucks, H.B. Schlegel, G.E. Scuseria, M.A. Robb, J.R. Cheeseman, G. Scalmani, V. Barone, G.A. Petersson, H. Nakatsuji, X. Li, M. Caricato, A.V. Marenich, J. Bloino, B.G. Janesko, R. Gomperts, B. Mennucci, H.P. Hratchian, J.V. Ortiz, A.F. Izmaylov, J.L. Sonnenberg, D. Williams-Young, F. Ding, F. Lipparini, F. Egidi, J. Goings, B. Peng, A. Petrone, T. Henderson, D. Ranasinghe, V.G. Zakrzewski, J. Gao, N. Rega, G. Zheng, W. Liang, M. Hada, M. Ehara, K. Toyota, R. Fukuda, J. Hasegawa, M. Ishida, T. Nakajima, Y. Honda, O. Kitao, H. Nakai, T. Vreven, K. Throssell, J.A. Montgomery Jr., J.E. Peralta, F. Ogliaro, M.J. Bearpark, J.J. Heyd, E.N. Brothers, K.N. Kudin, V.N. Staroverov, T.A. Keith, R. Kobayashi, J. Normand, K. Raghavachari, A.P. Rendell, J.C. Burant, S.S. Iyengar, J. Tomasi, M. Cossi, J.M. Millam, M. Klene, C. Adamo, R. Cammi, J.W. Ochterski, R.L. Martin, K. Morokuma, O. Farkas, J.B. Foresman, D.J. Fox, *Gaussian 16 Revision A.01, Gaussian Inc. Wallingford CT*, 2016.
[24] E.R. Johnson, S. Keinan, P. Mori-Sánchez, J. Contreras-García, A.J. Cohen, W. Yang, Revealing noncovalent interactions, J. Am. Chem. Soc. 132 (2010) 6498–6506, https://doi.org/10.1021/ja100936w.
[25] R.F.W. Bader, A quantum theory of molecular structure and its applications, Chem. Rev. 91 (1991) 893–928, https://doi.org/10.1021/cr00005a013.
[26] F. Weinhold, C.R. Landis, E.D. Glendening, What is NBO analysis and how is it useful? Int. Rev. Phys. Chem. 35 (2016) 399–440, https://doi.org/10.1080/0144235X.2016.1192262.
[27] S.T. Toenjes, J.L. Gustafson, Atropisomerism in medicinal chemistry: challenges and opportunities, Future Med. Chem. 10 (2018) 409–422, https://doi.org/10.4155/fmc-2017-0152.
[28] J.K.G. Watson, Vibrational Spectra and Structure a Series of Advances, Elsevier, New York, 1977.
[29] R.S. Ruoff, T.D. Klots, T. Emilsson, H.S. Gutowsky, Relaxation of conformers and isomers in seeded supersonic jets of inert gases, J. Chem. Phys. 93 (1990) 3142–3150, https://doi.org/10.1063/1.458848.
[30] S. Blanco, A. Lesarri, J.C. López, J.L. Alonso, The gas-phase structure of alanine, J. American Chem. Soc. 126 (2004) 11675–11683, https://doi.org/10.1021/ja048317c.
[31] R. Castillo, S. Blanco, J.C. López, Conformational isomerism in trans-3-methoxycinnamic acid: from solid to gas phase, Spectrochim. Acta A Mol. Biomol. Spectrosc. 311 (2024) 123997, https://doi.org/10.1016/j.saa.2024.123997.
[32] W. Gordy, R.L. Cook, Microwave Molecular Spectra, John Wiley & Sons, New York, 1984.
[33] A. Macario, J.C. López, S. Blanco, Molecular structure of salicylic acid and its hydrates: a rotational spectroscopy study, Int. J. Mol. Sci. 25 (2024) 4074, https://doi.org/10.3390/ijms25074074.
[34] A. Almenningen, O. Bastiansen, L. Fernholt, S.J. Cyvin, S.S. Cyvin, Structure and barrier of internal rotation of biphenyl derivatives in the Gaseous state, J. Mol. Struct. 128 (1985) 59–76.
[35] O. Bastiansen, L. Smedvik, Electron diffraction studies on fluoroderivatives of biphenyl, Acta Chem. Scand. 8 (1954) 1593–1598.
[36] W.I. Cross, N. Blagden, R.J. Davey, R.G. Pritchard, M.A. Neumann, R.J. Roberts, R. C. Rowe, A whole output strategy for polymorph screening: combining crystal structure prediction, graph set analysis, and targeted crystallization experiments in the case of diflunisal, Cryst. Growth Des. 3 (2003) 151–158, https://doi.org/10.1021/cg025589n.
[37] H.M. Berman, J. Westbrook, Z. Feng, G. Gilliland, T.N. Bhat, H. Weissig, I. N. Shindyalov, P.E. Bourne, The protein data bank, Nucleic Acids Res. 28 (2000) 235–242, https://doi.org/10.1093/nar/28.1.235.